PRESSURE VESSEL FRACTURE SAFETY INVESTIGATIONS USING AS CRITERION THE ONSET OF CRACK PROPAGATION

S. SAHGAL

Nordostschweizerische Kraftwerke AG (IVOK), Nuclear Power Plants Beznau, CH-5312 Döttingen, Switzerland

T. VARGA, M. JUNKER, M. SHAKESHAFT

Stress Analysis and Strength of Materials Research Department, Sulzer Bros. Ltd., CH-8401 Winterthur, Switzerland

SUMMARY

For the nuclear pressure vessel frangible behavior can be normally excluded. The critical material characteristic at fracture, K_{IC}, is with linear elastic fracture behavior of steels near to the onset of stable crack growth. With elastoplastic material behavior the onset point of the stable crack growth and the actual fracture may be well apart. The 5% secant method is here of little use. The onset point can be down to 60% of the P_{max}. As a lower bound criterion the onset of stable crack growth is proposed. This point is detected on RPV steel by acoustic emission method and confirmed with heat tinting tests.

From load at initiation of propagation P_i, the value of K_{Ii} can be derived. Similarly δ_i can be measured. For the purpose of measuring δ_i clip-in gauges were used according to the "Swiss guidelines for the measurement of COD". From the load/clip gauge displacement record, the load and clip gauge displacement at the onset of stable crack growth can be determined. These values are then used to calculate K_Q, K_{Ii}, δ_i and K_{ICD}. It is the purpose of this paper to show experimentally that in the elasto-plastic range a similarity exists between the critical crack sizes as determined by K_{Ii}, *COD*, J and equivalent energy methods.

Presented below (as an example) are few critical long surface defect depths a_c determined by different methods:

	σ	K_Q	a_C	K_{Ii}	a_C	δ_i^*	a_C^{**}
Head	250	172	130	266	305	0.4	325
Nozzle	550	172	27	266	65	0.4	58
Cylinder	350	172	65	266	160	0.4	153

σ in N/mm^2, K_Q, K_{Ii} in MN/m$^{3/2}$, δ_i and a_C in mm.

* A characteristic value measured by extrapolation to the fatigue crack tip.
** Using the value of $n = 1.8$ in the simplified strip yielding formula.

Discussion. — If all tensile stresses, i.e. mechanical, thermal and residual are taken into account, K_Q (and the still lower valid K_{Ic}) values are hardly suitable for the realistic determination of reactor pressure vessel fracture safety.

It is our opinion that a more realistic approach is the use of the onset of stable crack growth as a criterion. Both K_{Ii} and δ_i (J and also equivalent energy) demonstrate sufficient safety margins between the critical and tolerable defect sizes.

1. Introduction

In the early sixties the safety against frangible fracture of commercial light water pressure vessels was based solely on Charpy-V impact testing. The drop weight test according to ASTM E 208-66 for every forged component and the weld metal was introduced later. In order to evaluate the fracture safety of the nuclear pressure vessels manufactured according to the above criteria more thoroughly a fracture mechanics evaluation programme was envisaged.

A preliminary study [1] resulted in critical defect sizes in the order of magnitude of 10 mm and below (depth of the long surface crack). This was due to conservative fracture toughness estimates taken from the literature and the assumed residual stresses of 100 N/mm^2 to 150 N/mm^2.

To achieve a more realistic estimate of critical defect sizes and thus of safety against frangible fracture extended over life time, a fracture mechanics testing programme was worked out using specially instrumented CT-specimens of nearly true wall thicknesses and at temperatures determined taking the operational and radiation (NDTT shift) aspects into consideration.

2. Testing Material

Since a sufficient amount of the pressure vessel material was not available, it had first to be investigated as to how appropriate test material could be procured.

2.1 Choice and Procurement of Material

Material acceptance test data and welding procedure qualification tests showed, that the base metal exhibited the lowest impact toughness values and for the vessel of unit two (where the NDTT values were measured), also the highest NDT-temperatures. The vessel steel having no chromium as an alloying element, is not prone to underclad or heat affected zone cracking. As later investigations showed, no serious embrittlement occurs near the weldements. So the tests were restricted to base metal only.

The supplier of the pressure vessel steel prepared an analogous heat to special order and applied the same fabrication procedure and heat treatment. A sufficient analogy between the reactor pressure vessel steel and the latter could be demonstrated using tensile, impact and drop weight testing methods.

2.2 Material Properties

The test material 1.2 MD07, has the chemical composition as given in Table-I and the mechanical properties as shown in Fig. 1. The characteristic Charpy-V results can be seen in Fig. 2. Figs. 1 and 2 illustrate results of the heavier block with forged section of 660 x 280 x 3800 mm.

3. Fracture Mechanics Testing Programme

The fracture mechanics testing programme was dictated by the non availability of specific data for this steel at desired temperatures. Although low temperature K_{I_c} values have been established by Westinghouse [2] on small specimens, no evidence at higher temperatures was available. In consequence information on heavy section fracture behavior was lacking and no estimation of critical defect sizes at temperatures of interest was possible (For example the hydro tests are performed usually at 50 °C to 60 °C and according to pressure-temperature diagram the lowest temperature at which 20 % of nominal pressure is attained lies at about 200 °C).

Hence a testing programme in elasto-plastic range on heavy section specimen (6T and 10T) was initiated.

3.1 Specimens and Methods

The CT-specimens of 6T and 10T geometry were forseen representing different wall thickness array of the reactor pressure vessel. We were aware that neither the 5 % secant method nor K at P_{max} would deliver representative values of fracture thoughness under the given circumstances.

This led us to the need of defining an approperiate criteria and developing suitable experimental methods.

3.1.1 K at the Onset of Stable Crack Growth

As presented by one of the authors [3] at the IAEA-WG meeting the onset point of stable crack growth is a safe lower bound criterion. The initiation point departs more and more from P_Q point with increasing ductility. The detection of initiation point on heavy specimens where heat tinting is not applicable is problematic. It will be shown in Appendix A that acoustic emission method can be employed to detect the onset point.

Under the assumption that crack initiation takes place at max. load additional instrumented impact testing using fatigue precracked Charpy-V specimens was carried out.

3.1.2 COD at the Onset

To establish COD data at the onset of crack propagation (δ_i), the CT-specimens were instrumented using clip-in gauges in accordance with the methods described in [4] . The COD was determined at the tip (greatest length) of the fatigue precrack as shown in Fig. 3. The geometry and the fatigue conditions were in accordance with ASTM E 399-74. It has been shown by Stumpp, Varga, Boyle [5] that a good agreement exists between the clip-in gauge measurements and the results of the elasto-plastic finite element calculations.

4. Results

4.1 Critical Stress Intensity Values

P_Q, Load at the onset of stable crack growth and the max. load are summarised in Table 2. The computed values of K_Q and K_{I_i} are given in Table 3, K_{Q_i}, K_{I_c} and K_{I_d} values are illusterated in Fig. 4. The lower bound K_{I_i} values are about 50 % higher than the K_Q values determined by 5 % secant method. K_{I_i} was calculated at P_i, the force reading at the onset of stable crack growth.

4.2 Critical COD Value (δ_i)

The COD values at the initiation point and max. load are given in Tab. 2. In Fig. 5 the COD Values and clip-in gauge readings are shown. Fig. 5 also illustrates that the scatter between the clip-in gauge readings along the slit is rather small, one of the authors checked the curvature of the shown lines and found that the values computed by elasto-plastic finite element techniques also give similar results. The positions of the clip-in gauges in the IOT-CT-specimens can be seen in Fig. 6.

The values for fracture toughness were calculated using the following equations

$$K_{Qi} = (n \cdot \sigma_{0,2} \cdot E' \cdot \delta_i)^{1/2} \qquad (1)$$

$$K_{Q_{max}} = (n \cdot \sigma_{0,2} \cdot E' \cdot \delta_{max})^{1/2} \qquad (2)$$

The value of n can be taken as 1.0 for ductile, 1.8 for elasto-plastic and 2 for linear elastic behavior.

$$E' = \frac{E}{1 - \nu^2} \qquad \text{(for plane strain)}$$

$$E' = E \qquad \text{(for plane stress)}$$

4.3 J-Integral Method

The J-Integral values were calculated using the equation derived by Merkle and Corten [6]

$$J = \frac{\lambda_J \cdot A}{B \cdot b} \qquad (3)$$

where λ_J is a factor accounting for axial force and bending moment in a CT specimen. The value of λ_J varies between 2.31 and 2.55. The critical values of J were calculated at the point of crack initiation as a function of load point displacement, the crack length a was measured at the greatest length. Critical K-values based on J-Integral are summarized in Tab. 4 and Tab. 5

4.4 Equivalent Energy Method

Since the specimens were tested at temperatures for which valid K_{I_c} values (except in one case) in accordance with ASTM E 399-74 could not be obtained, the experimental results were further treated as in the work of Witt and Mager [7] , [8]. The $K_{I_{cd}}$ values were calculated using the equation

$$K_{I_{cd}} = K_{Bd} = \frac{b^2 \cdot P_B}{bd\ (2\ bd)^{1/2}} \cdot f\left(\frac{a}{W}\right)$$

The crack length a was measured at the greatest length and the displacement in the load displacement curve of the load points. The $K_{I_{cd}}$ values are included in the Table 4 and Tab. 5.

5. Critical Defect Sizes

Using the onset of the stable crack growth criterion and K values determined by different methods, the critical long surface crack depths and the critical circular shape internal defect diameters were computed and are given in Table 6. The safety margin can be expressed as a ratio between the critical and the actual defect size.

The usual inservice inspection US caliberation standard is a flat bottomed hole of 10 mm diameter. Fabrication tolerance level in Europe go down to 2 mm diameter, so under all conservative assumptions the safety factor is more than 10. This is valid even on nozzle regions where the max. stress has been assumed to be acting over the full section.

6. Conclusions

a. The onset point of the crack growth yields higher critical K values than 5% secant method.
b. To pinpoint the onset of crack growth acoustic emission technique is applicable provided sufficient calibration is made in advance.
c. Our usual approach i.e. beginning with the instrumented impact testing, continuing with LE quasi static measurements and finally elasto-plastic fracture testing with near true size specimens would give following picture:
   - Instrumented impact testing gives a good conservative estimate of K, if evaluated with equivalent energy method.
   - Linear elastic small specimen low temperature testing gives inadequate values. The near true wall thickness specimen seems to give a steeper elasto-plastic transition.

- The true elasto-plastic behaviour of vessel should be followed and evaluated with nearly true wall thickness specimens.

d. The obvious agreement between results of instrumented Charpy-V and quasi static testing may be due to similar effects of deformation rate and the size. In our opinion no general conclusion can be drawn.

e. The onset of stable crack growth criteria gives for the different methods applied similar defect sizes and sufficient safety margins.

The work reported above was performed at the Material Testing Laboratory of Sulzer Brothers, Switzerland and was sponsered by Nordostschweizerische Kraftwerke, Switzerland. The primary objective of this study has been to assess the facture safety of the pressure vessels of the Nuclear Power Plants Beznau I & II.

References

[1] Wiederholungsprüfungen der Reaktordruckgefässe Beznau, Vorstudie - 1. Teil. Junker, Lawina, Shakeshaft, Varga, Schiel.

[2] NOK Reactor Vessel Radiation Surveillance Program by S.E. Yanichko. WCAP-7214.

[3] Fracture Mechanics Applications: Implication of Detected Flaws. Report of a Specialists Meeting, Winterthur 3-5 Dec. 1975. IAEA-189.

[4] Prüfvorschriften für das COD Verfahren. Abteilung für die Sicherheit der Kernanlagen, ASK-AN-220, 12. Februar 1976.

[5] Experimental and Theoretical Analysis in Elastic-Plastic Fracture Mechanics. 2nd SMiRT Berlin 10-14 September 1974, by Stumpp, Varga, Boyle.

[6] Merkle and Corten, in Journal of Pressure Vessel Technology, Trans. ASME, Nr. 6, 1974 pp. 1-7.

[7] Buchalet and Mager, in ASTM STP 536 pp. 281-296

[8] Witt F.J, "The Equivalent Energy Method for calculating Elasto-Plastic Fracture". 4th National Symposium on Fracture Mechanics, Pittsburg 1971.

Appendix A

Acoustic Emission (Broad Outline)

The equipment used in these tests was a Laboratory Processor supplied by AET Corp, Model 201. The onset of stable crack growth was best observed by recording RMS values of the acoustic data. The transducer found best to suit our purposes was one with peak sensitivity at ca. 375 kHz. The signals were passed through a filter band of 250 to 500 kHz prior to registration. Best results were obtained by placing the transducer on the top surface of the specimen directly above the fatigue-crack front.

Stable crack growth initiation was recorded as either a significant increace in RMS value or by use of the floating-zero-threshold facility of the Model 201. A significant departure from the original zero threshold was found in many cases to coincide with the initiation of stable crack growth.

These suspected initiation points were always confirmed using the heat-tinting method on similar or smaller specimens of the same material. A schematic representation of acoustic emission during loading can be seen in Fig. 7.

Appendix B

The mashine used for testing consists of two halves with four horizontally mounted cylinder pushing them apart. The specimen is placed in the centre of the four columns and can be pulled with the maximum pulling force of 12 MN (1200 metric tons). Since the stroke of the mashine is 250 mm, it is possible to fracture with this mashine specimens with large plastic deformation in a single pull. This mashine can handle 4T- upto 14T-CT specimens and wide plates as well.
The load is measured with the caliberated strain gauges mounted on all four columns. The load is shown on a digital instrument and can be recorded too. The overall accuracy is about 2%. The kinetic energy of fast fractures is absorbed by compressing copper tubes of graded wall thicknesses.
Special care was taken for the temperature control. As shown in Fig. 8 6T and 10T-CT specimens were equiped with a number of thermocouples. Heating or cooling was started before mounting the specimen in the mashine and followed by in-situ treatment. For the latter a special heating and cooling chambers were built. A typical heating cycle for a 6T-CT probe geometry can be seen in Fig. 9.

TABLE I :

Chemical Composition (wt %) of Testing Material

Charge No.	C	Si	Mn	S	P	Cr	Ni	Mo	V	Cu	Nb	Co	Al	Ti
Poste 1 (10")	.172	.286	1.47	.0106	.016	.25	.87	.539	.012	.173	.01	.0298	.0363	.006
Poste 2 (6")	.175	.286	1.48	.0117	.016	.24	.86	.526	.012	.173	.01	.0278	.0401	.006

Dimensions of Poste 1: 660 × 280 × 3800 mm
Dimensions of Poste 2: 460 × 170 × 3040 mm

TABLE II :

Critical load and COD values as measured

Temperature	Specimen	Load			COD	
°C	Nr.	P_Q kN	P_i kN	$P_{max.}$ kN	δ_i mm	$\delta_{max.}$ mm
-42	H4 (10")	—	—	1'070	—	0.025
0	H1 (10")	3'870	4'920	5'080	0.45	0.60
+71	H2 (10")	3'530	5'220	5'470	0.60	0.90
0	H6 (6")	1'480	2'060	2'260	0.40	0.60
+31	H7 (6")	1'500	2'500	2'570	0.74	1.00
+70	H5 (6")	1'510	2'330	2'450	0.75	1.04

TABLE III :

Calculated Stress Intensity values ,

Temperature °C	Specimen Nr.	K-Values $[N \cdot mm^{-3/2}]$					
		K_{I_c}	$K_{Q_{ASTM}}$	K_{Q_i}	$K_{Q_{max.}}$	$K_{Q_{Si}}$	$K_{Q_{Smax}}$
-42	H4 (10")	1'980	—	—	1'980	—	2'510
0	H1 (10")	—	7'210	9'160	9'460	9'870	11'400
+71	H2 (10")	—	6'920	10'233	10'730	10'940	13'400
0	H6 (6")	—	5'540	7'710	8'460	9'550	11'700
+31	H7 (6")	—	5'580	9'300	9'560	12'690	14'760
+70	H5 (6")	—	5'640	8'700	9'140	9'390	11'060

TABLE IV :

Stress Intensity values computed in accordance with J-Integral and Equivalent Energy Methods for crack size $a = a_{max.}$ (max crack length)

Temperature °C	Specimen Nr.	K-Values $[N \cdot mm^{-3/2}]$			
		K_{J_i}	$K_{J_{max.}}$	$K_{I\,Cd_i}$	$K_{I\,Cd_{max.}}$
-42	H4 (10")				2'055
0	H1 (10")	10'535	11'083	11'012	11'585
+71	H2 (10")	12'450	14'640	13'484	15'864
0	H6 (6")	8'936	10'074	9'008	10'154
+31	H7 (6")	12'521	14'554	12'842	14'926
+70	H5 (6")	11'580	13'705	11'581	13'707

TABLE V :

Stress Intensity values computed in accordance with J-Integral and Equivalent Energy Methods for crack size $a = \bar{a}$

Temperature °C	Specimen Nr.	K-Values $[N \cdot mm^{-3/2}]$			
		K_{J_i}	$K_{J\,max.}$	$K_{I\,Cd_i}$	$K_{I\,Cd\,max.}$
-42	H4 (10")				1'962
0	H1 (10")	10'355	10'895	10'209	10'761
+71	H2 (10")	12'218	14'363	12'669	14'905
0	H6 (6")	8'831	9'955	8'735	9'847
+31	H7 (6")	12'379	14'384	12'356	14'366
+71	H5 (6")	11'467	13'571	11'433	13'304

TABLE VI :

Critical defect sizes (for nozzle region) determined by different methods.
$\sigma' = 550\ N/mm^2$ and $\sigma_{0.2} = 500\ N/mm^2$

	$N \cdot mm^{-3/2}$	Surface Defect $\frac{a}{2c} = 0.1$	Internal Defect $\frac{a}{2c} = 0.5$		$N \cdot mm^{-3/2}$	Surface Defect $\frac{a}{2c} = 0.1$	Internal Defect $\frac{a}{2c} = 0.5$
$K_Q \quad (a=\bar{a})$	7'210	40 • 400	123				
$K_{Q_i} \quad (a=\bar{a})$	9'160	65 • 653	198	$K_{COD_i}^{(a=a_{max})}$	9'870	76 • 760	230
$K_{J_i} \quad (a=\bar{a})$	10'355	83 • 830	253	$K_{J_i}^{(a=a_{max})}$	10'535	86 • 860	262
$K_{Icd_i} \quad (a=\bar{a})$	10'209	81 • 810	246	$K_{Icd_i}^{(a=a_{max})}$	11'012	94 • 940	286
$K_{Q_{max}} \quad (a=\bar{a})$	9'460	70 • 700	211	$K_{COD_{max}}^{(a=a_{max})}$	11'400	101 • 1010	306
$K_{J_{max}} \quad (a=\bar{a})$	10'895	92 • 920	280	$K_{J_{max}}^{(a=a_{max})}$	11'083	96 • 960	290
$K_{Icd_{max}} \quad (a=\bar{a})$	10'761	90 • 900	273	$K_{Icd_{max}}^{(a=a_{max})}$	11'585	104 • 1040	316

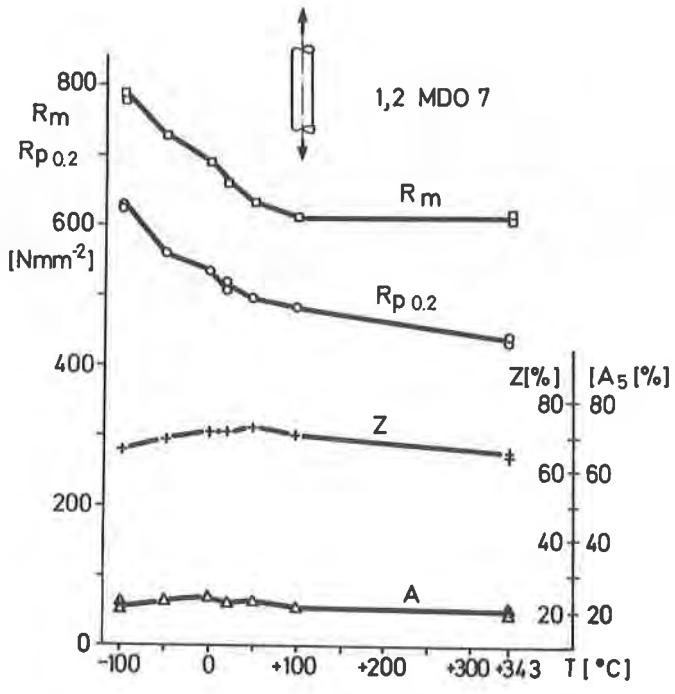

Fig. 1 : Tensile properties of the testing material 1,2 MDO 7 in function of temperature. R o.2: Yield Strength; R_m: Ultimate Strength; Z: Reduction of Area and A: Elongation.

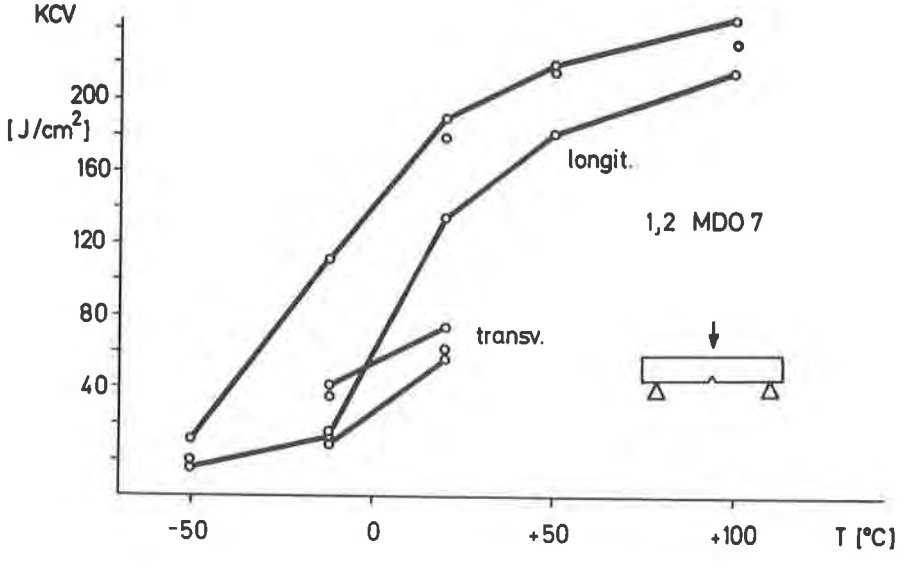

Fig. 2 : Charpy - V Transition

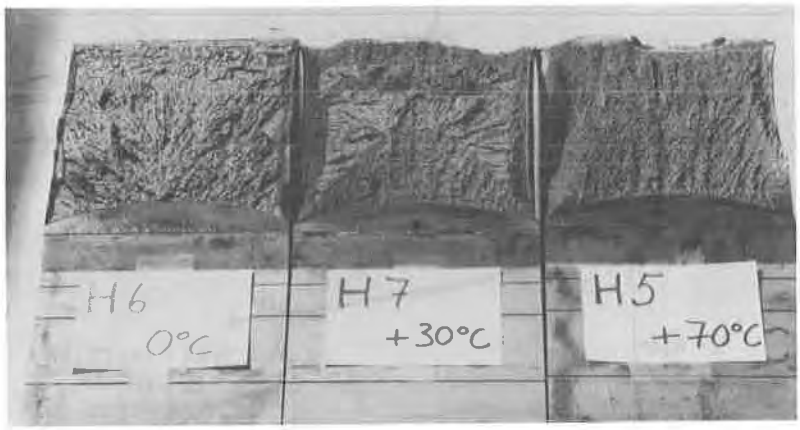

Fig. 3 : Fracture surfaces 6T-CT specimens. The crack length was measured at the greatest length.

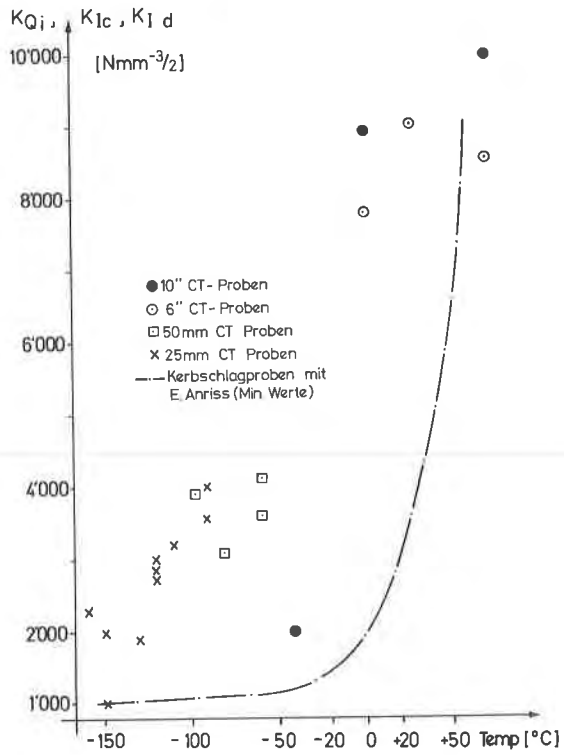

Fig. 4 : K_Q at initiation of stable crack growth, K_{I_c} and lower bound of precracked Charpy specimens (impact test) in function of temperature.

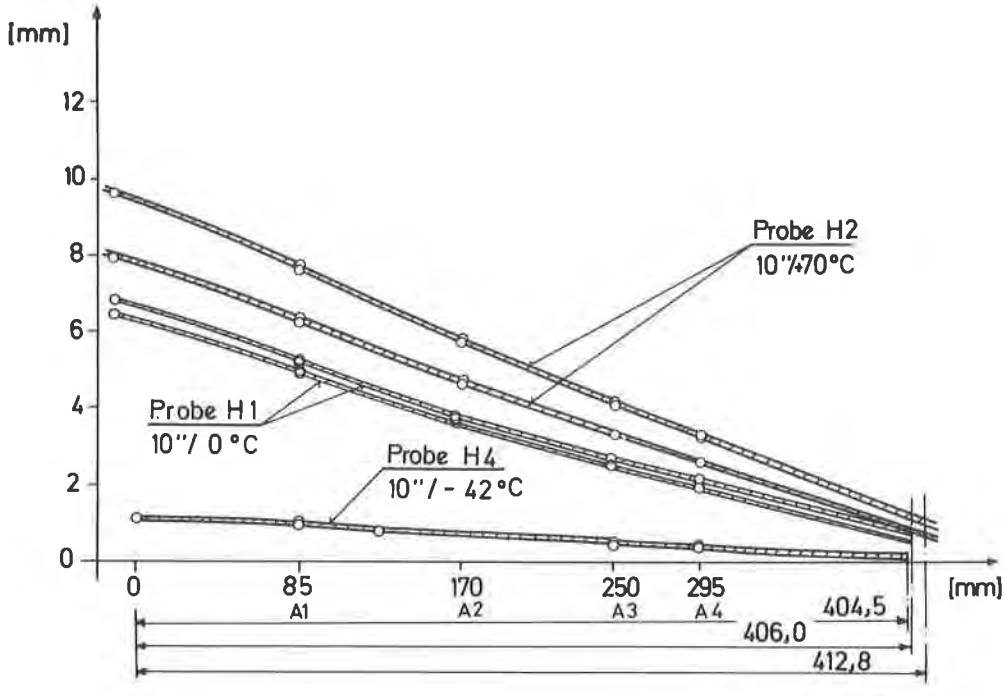

Fig. 5 : Clip-in gauge readings at different temperatures and positions on a 10T-CT specimen.

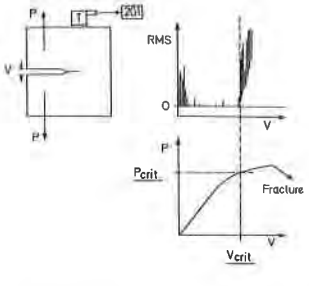

Fig. 6 : Clip-in gauge positions in the 10T-CT specimen.

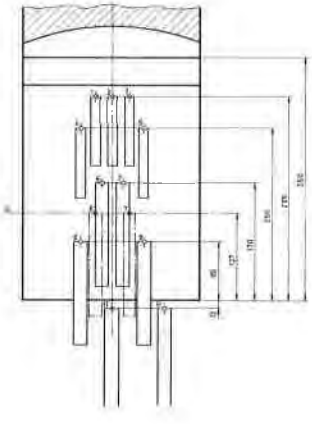

Fig. 7 : Schematic representation of acoustic emission during specimen loading.

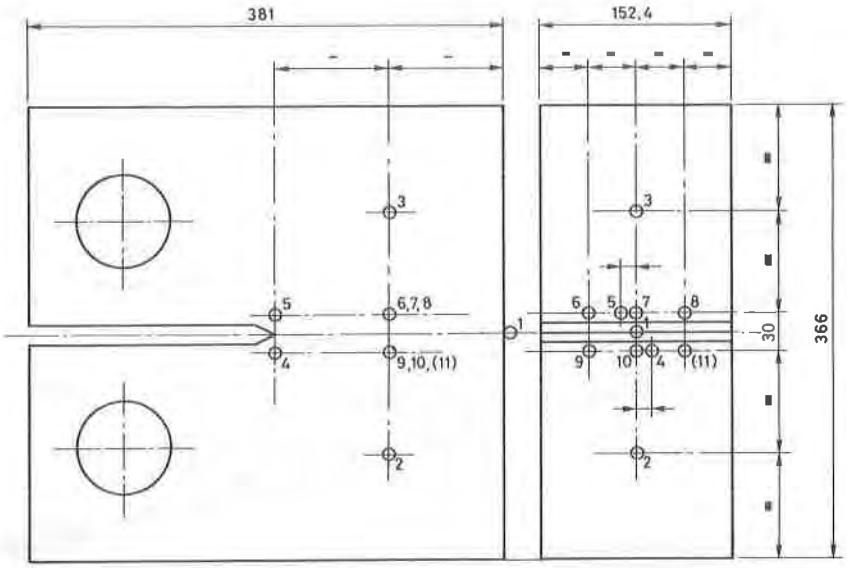

Fig. 8 : Position of thermocouples in a 6T-CT specimen

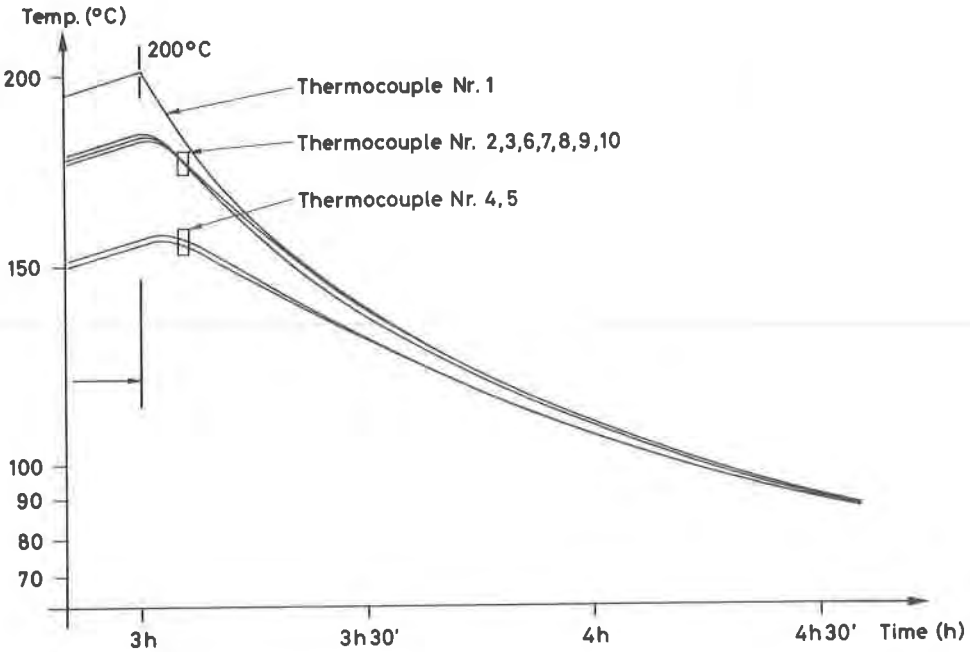

Fig. 9 : Temperature versus time curves for different thermocouples (shown in Fig. 9). The peak temperature being 200°C.